Journal of Materials Science: Materials in Electronics (2019) 30:20614–20623
https://doi.org/10.1007/s10854-019-02427-1

# Effect of $Al_2O_3$ on microstructure and dielectric properties of epoxy-cyanate ester composite material

Yufei Chen[1,2,3] · Zhiguo Li[1] · Yulong Liu[1] · Chengjun Teng[4] · Weiwei Cui[1]

Received: 13 July 2019 / Accepted: 21 October 2019 / Published online: 29 October 2019


## Abstract

The bisphenol A epoxy resin (E51) and biscyanatophenylpropane (BCE) were used as polymer matrix, $Al_2O_3$ (self-made with sol–gel method) as modified agent to prepare $Al_2O_3$/E51-BCE composites, and the thermal stability and dielectric properties of the composites were studied. FT-IR and transmission electron microscope (TEM) of $Al_2O_3$ showed that $Al_2O_3$ was short fiber-shaped crystal with hydroxyl groups on its surface. Scanning electron microscope (SEM) and energy-dispersive spectrum (EDS) analysis of $Al_2O_3$/E51-BCE composites indicated a strong interaction between $Al_2O_3$ and E51-BCE matrix resin, and the surface of the two phases was fuzzy. $Al_2O_3$ dispersed uniformly in the E51-BCE matrix as the dispersed phase. The interface among phases was blurred and showed a mutual penetrating phenomenon. Furthermore, the cross section of cracks was rough and the directions changed. This is a typical ductile fracture morphology. The highest value of the breakdown strength and volume resistivity of the $Al_2O_3$/E51-BCE composites were 15.1 kV/mm and $1.53 \times 10^{15}$ Ω m, which was 13.5% and 86 times higher than that of the E51-BCE matrix, respectively, when the content of $Al_2O_3$ was 3 wt%. And the dielectric constant and dielectric loss tangent of the composite materials were 3.73 and 0.0029 at the electric field frequency of 100 Hz. Thermogravimetric curves displayed that the introduction of $Al_2O_3$ slightly decreased the thermal decomposition temperature during the range of 0 ~ 5 wt% $Al_2O_3$, but the thermal decomposition temperature of $Al_2O_3$/E51-BCE composites was all over 400 °C; the composite materials still had high heat resistance. Overall, this study facilitates the applications of $Al_2O_3$/E51-BCE composites in a broad range of fields.

## 1 Introduction

Cyanate ester resin (CE) is one of the most important thermosetting resins, due to its many outstanding properties, including low water absorptivity, high heat resistance and glass transition temperature, low dielectric constant and dielectric loss [1–3]. CE is currently used in electronics packaging, aerospace structural components, adhesives and missile materials [4, 5]. CE monomer contains two or more cyanate groups with high activity; they can form triazine ring structure by the action of heat or catalyst. However, the triazine rings are highly symmetrical molecular structure, which makes the CE materials easy crystallizing and brittle, limiting the application of CE in dielectric materials field [6–9]. To overcome the drawbacks of CE in toughness, the epoxy resin (EP) has become an ideal toughening modification material to CE for its flexible molecular structure, high reaction activity and similar processability with CE [10, 11]. However, the EP has limited improvement effect of CE on dielectric properties and thermal stability [12, 13]. In view of this, the nano-$Al_2O_3$ is chosen as the inorganic

✉ Yufei Chen
chenyufei@hrbust.edu.cn

Zhiguo Li
lizhiguomy@gmail.com

Yulong Liu
375976129@qq.com

Chengjun Teng
810025406@qq.com

Weiwei Cui
cuiww@hrbust.edu.cn

1 School of Materials Science and Engineering, Harbin University of Science and Technology, Harbin 150040, China

2 Key Laboratory of Engineering Dielectrics and Its Application, Ministry of Education, Harbin University of Science and Technology, Harbin 150080, China

3 Key Laboratory of Advanced Manufacturing and Intelligent Technology, Ministry of Education, Harbin, China

4 Harbin Xiangfang District Center for Disease Control and Prevention, Harbin 150030, China

reinforcement to modify the blending resin of CE and EP, because the large surface area and small size effect of nano-$Al_2O_3$ have significant impact on the electrical properties, heat resistance and mechanical properties of the resin materials [14–16].

At present, there are few reports on the dielectric properties of cyanate resin systems modified by nano-$Al_2O_3$. In this paper, nano-$Al_2O_3$ prepared by sol–gel method was used as a reinforcement, and a copolymer of CE and epoxy resin as the matrix resin to prepare a composite material with high dielectric properties and thermal stability. And then the composites were characterized and analyzed the effects of nano-$Al_2O_3$ on the electric breakdown behavior and dielectric properties of the composites. This paper will provide reference for the preparation of high-performance insulating materials and broadens the application fields of cyanate ester resin.

## 2 Experimental

### 2.1 Materials

Biscyanatophenylpropane (BCE) purchased from Yangzhou Technical Material Co., Ltd. Bisphenol A epoxy resin (E51, epoxy value of 0.51) was industrial products and provided by Nantong Xingchen Synthetic Material Co., Ltd. Aluminum isopropoxide was purchased from Tianjin Fuchen Chemical reagent factory, chemically pure. Isopropanol was purchased from Dongguan Spartan Reagent Co., Ltd, analytical pure.

### 2.2 Preparation of $Al_2O_3$

Aluminum isopropoxide, isopropanol and deionized water were stirred in a water bath to sufficiently hydrolyze aluminum isopropoxide at 80 °C for 2 h. The isopropanol and deionized water were removed in reduced pressure distillation, and the solid was dried at 120 °C and calcined at 700 °C for 3 h to obtain $Al_2O_3$. The preparation process was shown in figure below (Fig. 1).

### 2.3 Synthesis of E51-BCE matrix resin

The mass ratio of E51 to BCE was set to 2:8. BCE resin was added to E51 resin preheated to 90 °C. Then the mixed system was heated to 120 °C and kept for 1 h. After that, the mixed system was poured into a mold which had been preheated to 140 °C and cured at 180 °C/4 h + 200 °C/2 h to obtain a modified cyanate material (E51-BCE).

### 2.4 Preparation of $Al_2O_3$/E51-BCE composites

$Al_2O_3$ was added into E51 and ultrasonically dispersed for 1 h at 80 °C; BCE was added into above system to prepare $Al_2O_3$/E51-BCE composites, according to 180 °C/4 h + 200 °C/2 h procedure. The content of $Al_2O_3$ in composites was 1 wt%, 3 wt% and 5 wt%, respectively. The process was shown in figure below (Fig. 2).

### 2.5 Measurements

The Fourier-transform spectrometer (FT-IR, EQUINOX-55, Germany) is used to determine the absorption peak of the substance and analyze the presence of the group in the range of 400 ~ 4000 $cm^{-1}$, and five scans are tested for each sample.

Thermogravimetric analysis (TGA), which not only could investigate the status of a material and the process of decomposition but also can provide useful information about the thermal stability of material, is recorded on a PekinElmer 6 series thermal analysis system (USA), samples are heated from 200 °C to 800 °C at the heating rate of 20 °C·$min^{-1}$ in a nitrogen atmosphere, and the weight of sample is about 10–15 mg.

The status of aggregation and morphology of $Al_2O_3$ are tested by JEM-2100 transmission electron microscopy

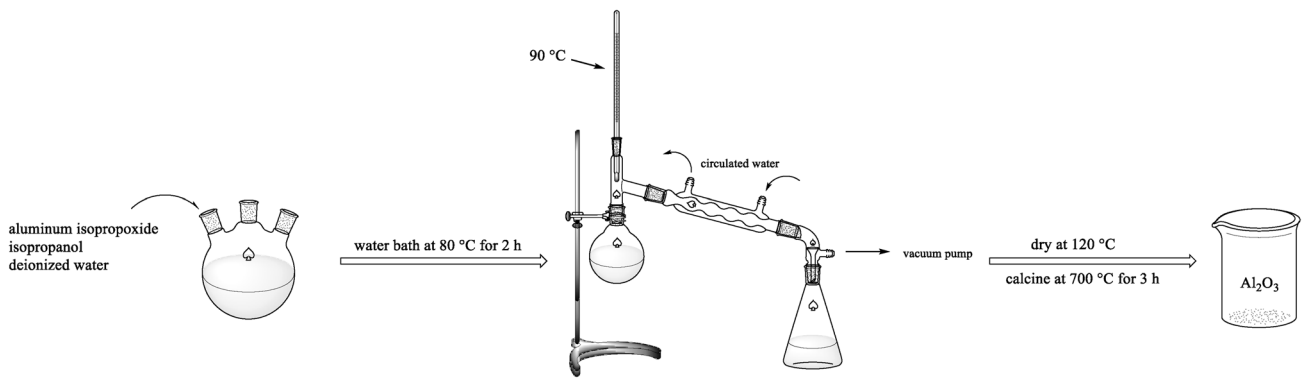


**Fig. 1** The preparation process of $Al_2O_3$ with sol–gel method

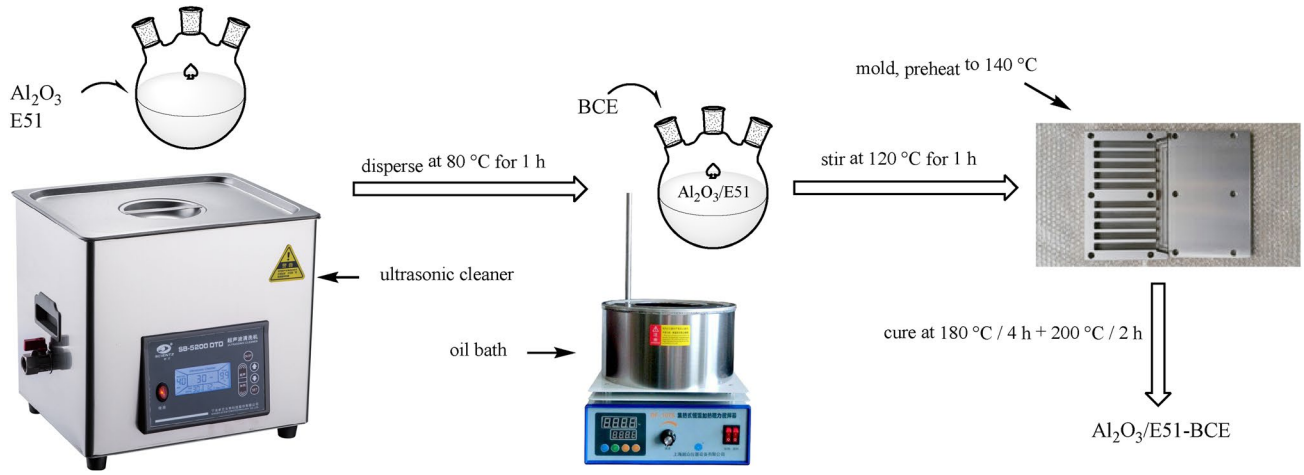


**Fig. 2** The preparation process of $Al_2O_3$/E51-BCE composites

(TEM, Japan); the test temperature is 18 °C and voltage is 120 kV.

The fracture micro-morphology of the composite materials and the breakdown holes are observed using a Sigma 500 scanning electron microscope (SEM, ZEISS, Germany). The samples are deposited on a sample holder with adhesive carbon foil and sputtered with gold before being examined. And the Jupiter 5000 radiation shielded X-ray tube (Oxford Instruments) was used as the X-ray source for energy-dispersive spectrum (EDS).

The dielectric constant ($\varepsilon$) and dielectric loss (tan$\delta$) of the composite materials are measured with Agilent-4294A precise impedance analyzer (Japan) in the frequency range of 100 Hz ~ 100 kHz at room temperature according to GB/T 1409-2006.

The volume resistivity of the composites is tested with a ZC-36 high resistance meter (Shanghai Precision Instruments Co., Ltd), and the tests are carried on at room temperature.

The breakdown strength of the composites is measured with a CS2674C dielectric strength tester (Nanjing) in silicone oil and at room temperature, according to GB/T 1408-89. The rate of voltage is 1 kV/s.

## 3 Results and discussions

### 3.1 Microstructure of $Al_2O_3$ and $Al_2O_3$/E51-BCE composites

#### 3.1.1 FT-IR spectra of $Al_2O_3$ and $Al_2O_3$/E51-BCE composites

Figure 3 presents the FT-IR spectra of $Al_2O_3$ and $Al_2O_3$/E51-BCE composites. From Fig. 3, it can be seen that

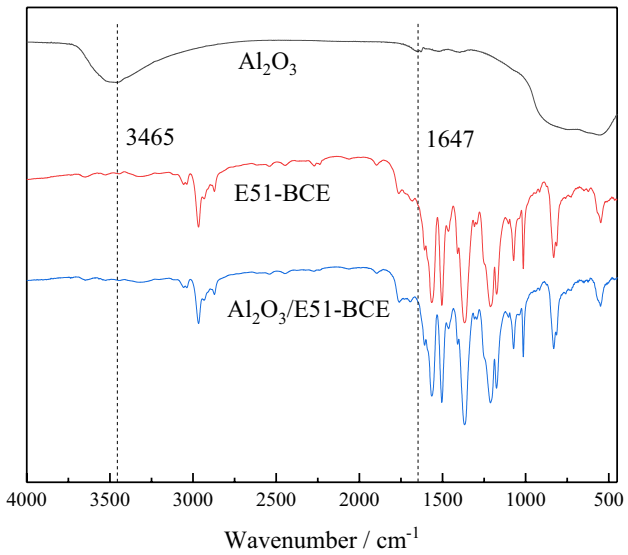


**Fig. 3** FT-IR spectra of $Al_2O_3$ and $Al_2O_3$/E51-BCE composites

$Al_2O_3$ exhibits the infrared absorption peaks at 3465 and 1647 $cm^{-1}$, which are the characteristic peaks of hydroxyl groups and hydrogen bonding via inter- or intra-nanoparticles surface interaction, respectively [17–19]. These two infrared absorption peaks disappear after the $Al_2O_3$ is mixed with the E51-BCE matrix resin (in the curve of $Al_2O_3$/E51-BCE), this could be an evidence to prove that the interaction between the $Al_2O_3$ particles is weakened and chemical bonding or chemical absorption is formed between the $Al_2O_3$ and the matrix resin via the hydroxyl groups. The chemical bonding or chemical absorption will produce a strong interface interaction and contribute to improving the properties of composite materials [20].

#### 3.1.2 TEM images of $Al_2O_3$

It can be seen from Fig. 4 that the $Al_2O_3$ is a short fiber-shaped crystal with a dimension of about 50 nm in length and 5 nm in diameter; nano-sized $Al_2O_3$ could be beneficial to improve the dielectric properties of the composite materials, due to its small size effect, interfacial effect and chemical bonding with the matrix resin. These factors will influence the properties of the composite materials in following ways: (1) a large interface area is formed between $Al_2O_3$ and the matrix resin due to the high specific surface area of the nanoparticles, which creates a large interaction zone [21, 22]; (2) the reduction in size causes the internal electric field to reduce and the space charge to change [23, 24]; (3) the hydroxyl groups on the surface of $Al_2O_3$ contribute to improving the compatibility of $Al_2O_3$ with the matrix resin [19].

#### 3.1.3 SEM analysis of $Al_2O_3$/E51-BCE composites

SEM is usually used to indicate the fracture morphology of the composites and the dispersity of inorganic component in the polymer matrix. The fracture morphologies of $Al_2O_3$/E51-BCE composites are studied by using SEM, as shown in Fig. 5, and the EDS of the fracture surface is shown in Fig. 6. For the E51-BCE material (Fig. 5a), it can be seen that the fracture surface is basically regular and smooth; the broken cracks present a single-directional development, which basically conforms with the brittle fracture characteristics [25, 26]. This is because the internal structure of the E51-BCE matrix resin is still regular and there is no obstruction when the material is subjected to external forces; the cracks expand in one direction to make the cracks progress smoothly along the stress direction [27]. In Fig. 5b–d, the fracture surface morphology of the composites has emerged the difference with Fig. 5a due to the presence of $Al_2O_3$ component, and irregular cracks have appeared. The fracture surface of the composites exhibits short and disorderly cracks when the content of $Al_2O_3$ reaches 3 wt%, as shown in Fig. 5c. $Al_2O_3$ evenly disperses in the matrix resin, and the strong interaction makes the crack directions of composite materials change and present arborization when the composite is subjected to external forces, making the fracture behavior exhibit ductile fracture [28, 29]. Many microcracks have formed and absorb the fracture energy, and the shear zones are induced by $Al_2O_3$ particles when the interaction between the two phases is stronger. However, due to the enhanced interaction between the $Al_2O_3$ particles (read mark in Fig. 6), agglomeration phenomenon of $Al_2O_3$ component occurs and the diameter of $Al_2O_3$ is relatively bigger when its content is more than 3 wt%, which can be confirmed in Fig. 6. The agglomeration of $Al_2O_3$ makes the interfacial interaction diminish, and its negative effect on the material performances can be confirmed in the following content.

### 3.2 Thermal stability of $Al_2O_3$/E51-BCE composites

Figure 7 shows the thermogravimetric curves of the $Al_2O_3$/E51-BCE composites, and the thermal decomposition temperature ($T_d$) is exhibited in Table 1, in which $T_d^5$ and $T_d^{10}$ indicate

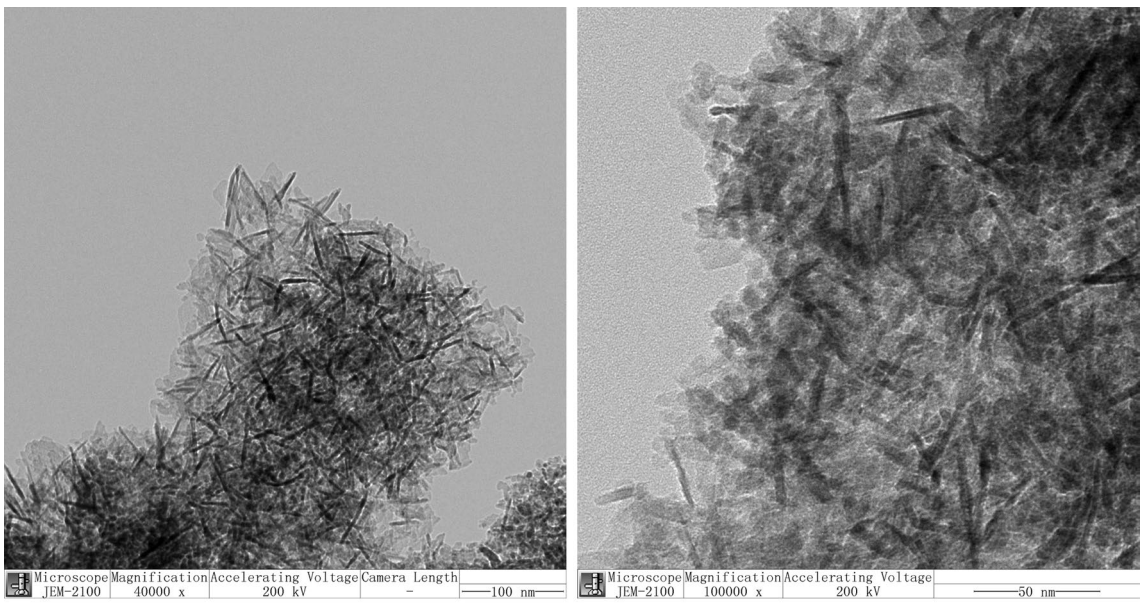


a b

**Fig. 4** TEM images of $Al_2O_3$. **a** 40000x, **b** 100000x

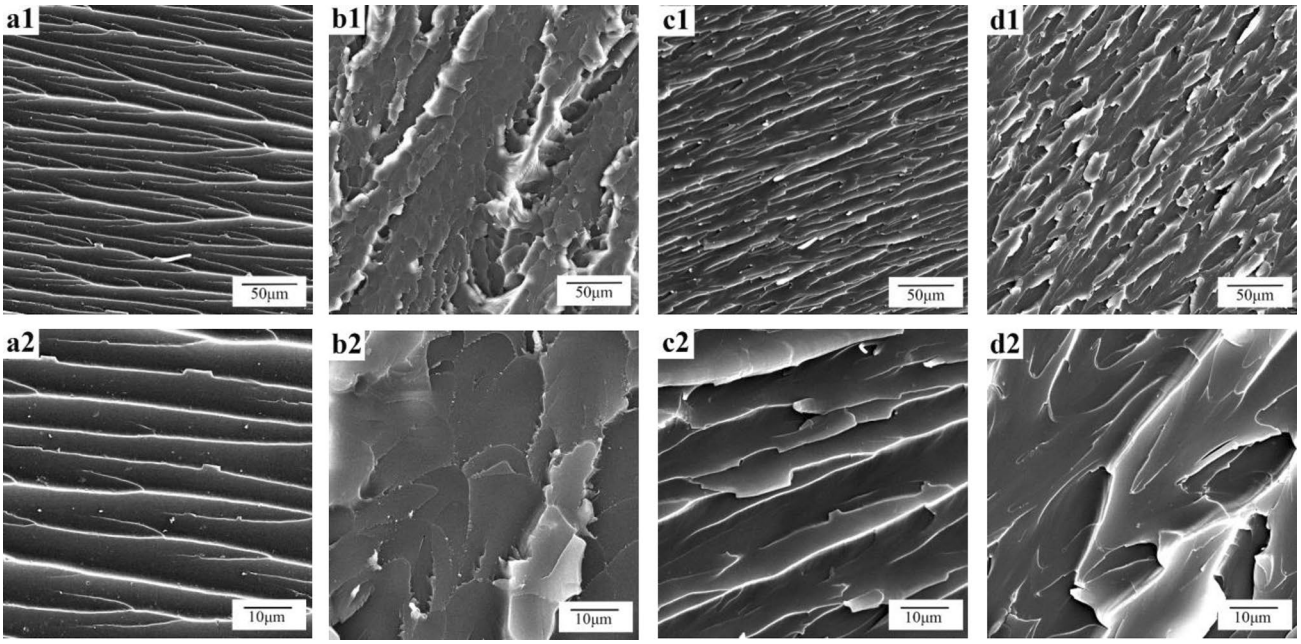


**Fig. 5** SEM images of $Al_2O_3$/E51-BCE composites: **a1**, **a2** E51-BCE, **b1**, **b2** 1 wt% $Al_2O_3$/E51-BCE, **c1**, **c2** 3 wt% $Al_2O_3$/E51-BCE, **d1**, **d2** 5 wt% $Al_2O_3$/E51-BCE

$T_d$ at 5 wt% and 10 wt% mass loss fractions, respectively. It can be seen from Fig. 7; Table 1 that the $T_d$ of the composite materials decreases slightly, with the increase in $Al_2O_3$ content. This result does not conform to the general law of the resin matrix composites modified by inorganic nanoparticles. This may be because the heat resistance of the E51-BCE matrix resin mainly comes from the high cross-linking density and the stable triazine ring structure [30, 31], the molecular chains are restricted to thermally vibrate, and the decomposition of the molecular chains requires a large amount of energy [32, 33]. The introduction of $Al_2O_3$ may reduce the cross-linking density of the resin matrix, so is the restriction to thermal vibration of the molecular chains [34, 35]; it could also reduce the thermal decomposition activation energy of the matrix resin [36]. All these factors work together, making $T_d$ of the $Al_2O_3$/E51-BCE composites lower than that of the E51-BCE matrix resin. As for the composite materials with 5 wt% $Al_2O_3$, the small size effect and interfacial effect of $Al_2O_3$ have failed due to its aggregation, and the effect of $Al_2O_3$ on the cross-linking density of the matrix resin weakens [37]. Still, $Al_2O_3$ particles have little effect on the heat resistance of composite materials and do not affect heat resistance grade of the composites.

## 3.3 Dielectric properties of $Al_2O_3$/E51-BCE composites

### 3.3.1 Dielectric constant

Figure 8 displays the dielectric constant of $Al_2O_3$/E51-BCE composites in the frequency range of $10^2$ Hz ~ $10^6$ Hz. It can be seen that the dielectric constant of the composite materials conforms to the general characteristics of the frequency dependence of the thermosetting resin material on the electric field. The dielectric constant of the composite materials slightly decreases with the increasing frequency when the frequency is less than $10^4$ Hz, this is because the dipoles inside the composite materials can keep up with the change of electric field in the low-frequency region and the steering polarization is strong [38]. And, in the high frequency region ($10^4$ Hz to $10^6$ Hz), the dipoles cannot be consistent with the alternating electric field due to the influence of the internal viscous effect, caused by the high cross-linking density of the E51-BCE resin matrix [39, 40]. The dipoles keep in the status of relaxation, and the steering polarization is hard to establish; this makes the steering polarization

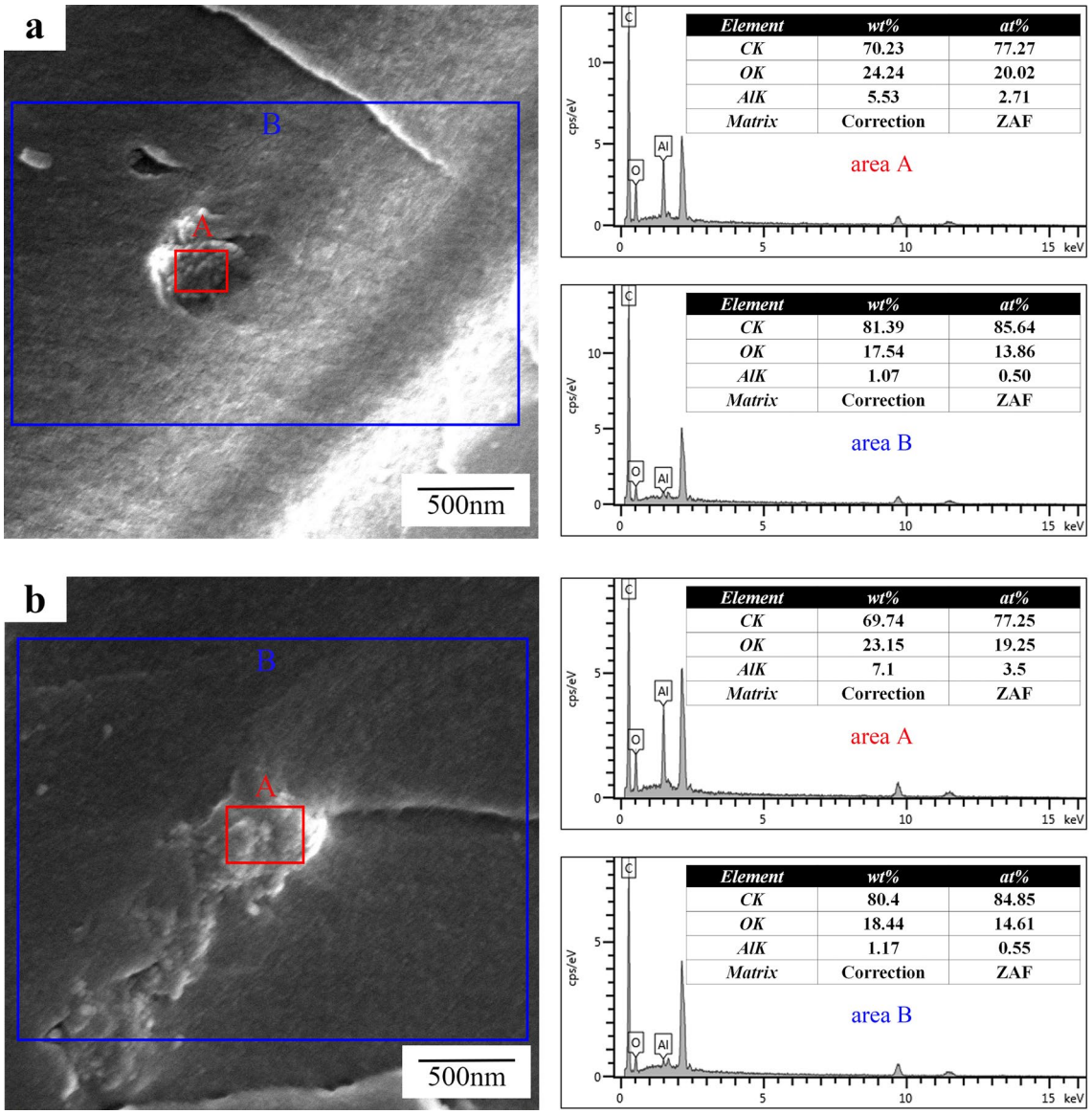


**Fig. 6** SEM and EDS images of 3 wt% $Al_2O_3$/E51-BCE (**a**) and 5 wt% $Al_2O_3$/E51-BCE (**b**)

reduce [41, 42]. And then, it can also be seen from Fig. 8 that $Al_2O_3$ can effectively reduce the dielectric constant of the composite materials, and the higher the $Al_2O_3$ content, the lower the dielectric constant of the composites. The dielectric constant of the material is 3.73, when the content of $Al_2O_3$ is 5 wt%, and the alternating electric field frequency is 100 Hz. This may be because $Al_2O_3$ uniformly disperses in the matrix resin when the content of $Al_2O_3$ is appropriate, which forms a large number of interfaces between the matrix and the $Al_2O_3$ [43]. These interfaces restrict the movement of macromolecular chains and the lattice vibration of the E51-BCE matrix resin, so is the steering polarization of the $Al_2O_3$ in alternating electric field [25]. The negative effect of $Al_2O_3$ polarity on the decrease in dielectric constant of the composites is suppressed, and the dielectric constant of the composite materials reduces.

### 3.3.2 Dielectric loss

The dependence of the dielectric loss of $Al_2O_3$/E51-BCE composites on electric field frequency and $Al_2O_3$ content is presented in Fig. 9. It can be clearly seen that the dielectric loss of the composite materials increases with the increasing frequency ($10^2$ Hz ~ $10^6$ Hz), and the curves show a maximum slope in the range of $10^4$ Hz ~ $10^5$ Hz. Due to the effect of internal viscous and friction forces, the establishment of the dipole steering polarization will absorb lots of electric field energy and convert it into heat, resulting in the increase

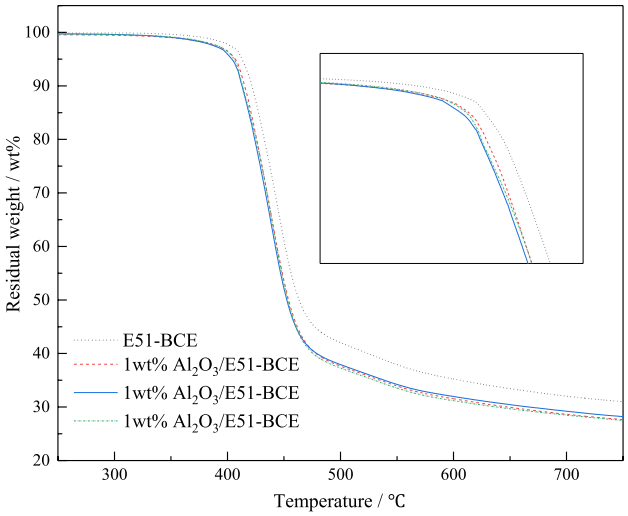


**Fig. 7** TGA curves of $Al_2O_3$/E51-BCE composites

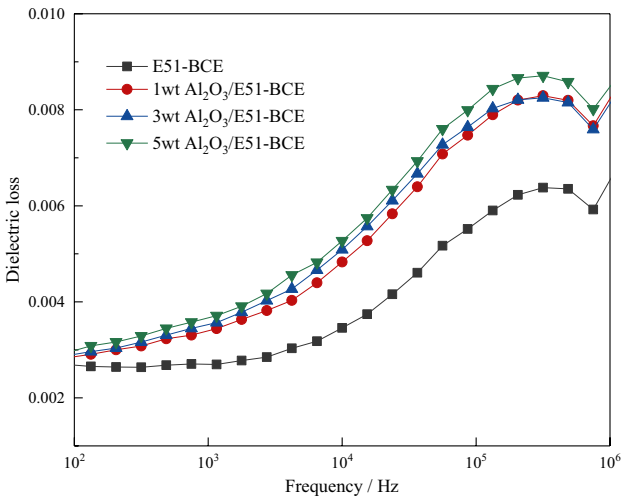


**Fig. 9** Dielectric loss of $Al_2O_3$/E51-BCE composites

**Table 1** Thermal decomposition temperature of $Al_2O_3$/E51-BCE composites

| Component | $Al_2O_3$ content/wt% | $T_d$/ °C | $T_d^5$/ °C | $T_d^{10}$/ °C |
|---|---|---|---|---|
| E51-BCE | 0 | 410.8 | 413.1 | 421.6 |
| $Al_2O_3$/E51-BCE | 1 | 408.5 | 406.9 | 415.2 |
| $Al_2O_3$/E51-BCE | 3 | 405.5 | 403.8 | 412.9 |
| $Al_2O_3$/E51-BCE | 5 | 406.8 | 405.9 | 413.3 |

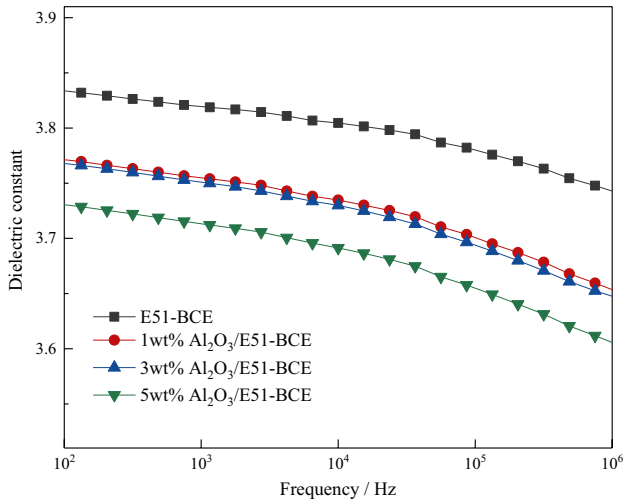


**Fig. 8** Dielectric constant of $Al_2O_3$/E51-BCE composites

in dielectric loss [44]. And, as the frequency of the electric field increases, the electric field energy consumed by dipole steering polarization also increases rapidly [45]. So, the dielectric loss increases with the increasing electric field frequency. However, same as the dependence of dielectric constant on the electric field frequency, if the frequency of the electric field is high enough (over $10^5$ Hz), the dipoles inside the composite materials keeps in the process of relaxation for they have no enough time to establish the steering polarization. In this case, the electric field energy consumed in overcoming the internal viscous and friction forces is reduced, and this change is macroscopically represented as a decrease in the dielectric loss. [16, 46].

The dielectric loss tangent of the composite materials is between 0.002 and 0.009 in the frequency of $10^2 \sim 10^6$ Hz, and dielectric loss tangent of the composite materials is 0.0029 when the content of $Al_2O_3$ is 5 wt% at 100 Hz. By observing Fig. 9, the introduction of $Al_2O_3$ makes the dielectric loss tangent of the composites increase and the effect of $Al_2O_3$ on the dielectric loss of the composite materials mainly reflects in the high-frequency region. It is supposed that $Al_2O_3$ is electrostatically or chemically bonded to form a strong interfacial function with the matrix resin, which helps to reduce the dielectric constant of the material. However, $Al_2O_3$ itself has a high polarity; dielectric loss is generated by the steering polarization of $Al_2O_3$ due to the action of the alternating electric field. Since the rate of polarization of $Al_2O_3$ is higher than that of the matrix resin, both the $Al_2O_3$ and the matrix resin can rapidly complete the polarization process in the low-frequency alternating electric field; in this case, the introduction of $Al_2O_3$ has no significant effect on the dielectric loss of the composites [47]. And in the high-frequency region, the $Al_2O_3$ turns frequently with the alternating electric field to make the dielectric loss much higher than that of the matrix resin [48]. Also, a strong interaction and the frictional resistance between $Al_2O_3$ and matrix resin will be overcome, resulting in increasing conductance loss during the movement process of the trace amount of

conductive carriers inside the composites. Meantime, the higher the asymmetry of two-phase interface polarity, the higher the dielectric loss, due to the interfacial polarization function of the composite materials.

### 3.3.3 Breakdown strength and volume resistivity

Breakdown of insulating material generally generates thermal breakdown and electrical breakdown at the breakdown point, and as the breakdown happens, the electric energy is converted into thermal energy and the composites are destroyed. Figure 10 exhibits the SEM images of breakdown holes of 3 wt% $Al_2O_3$/E51-BCE composites and E51-BCE matrix resin. In Fig. 10a, b, there is a ring-shaped ablation area around the breakdown hole and produce the partial discharge, which conforms to the general characteristic of corona discharge [49]. It can be considered that a little amount of water or air gaps on the surface of the composites is ionized in the strong electric field, and these ions accelerate in the direction of electric field and bombard the composites surface to make the electric energy convert into heat energy, so the polymer matrix is thermally decomposed and a corona ring formed [50, 51]. In Fig. 10c, d, compared with the E51-BCE matrix resin, the composites with $Al_2O_3$ particles show more branches on the breakdown channel and secondary branches, indicating that incorporating $Al_2O_3$ can help to enhance the scattering of carriers. These branches consume lots of kinetic energy of the carriers and improve the properties of voltage resistance.

Figure 11 shows SEM images and the EDS of the composite's breakdown hole, in which the content of $Al_2O_3$ is 3 wt%. The result of EDS indicates that the aluminum atom content on the branch surface is extremely low, which suggests that the dispersiveness between two phases is very well and inorganic $Al_2O_3$ may disperse in matrix. This phenomenon will improve the performances of the composites.

The breakdown strength and volume resistivity of $Al_2O_3$/E51-BCE composites are exhibited in Table 2, and the composites show the peak value of 15.1 kV/mm and $1.53 \times 10^{15}$ Ω m when the content of $Al_2O_3$ is 3 wt%, which

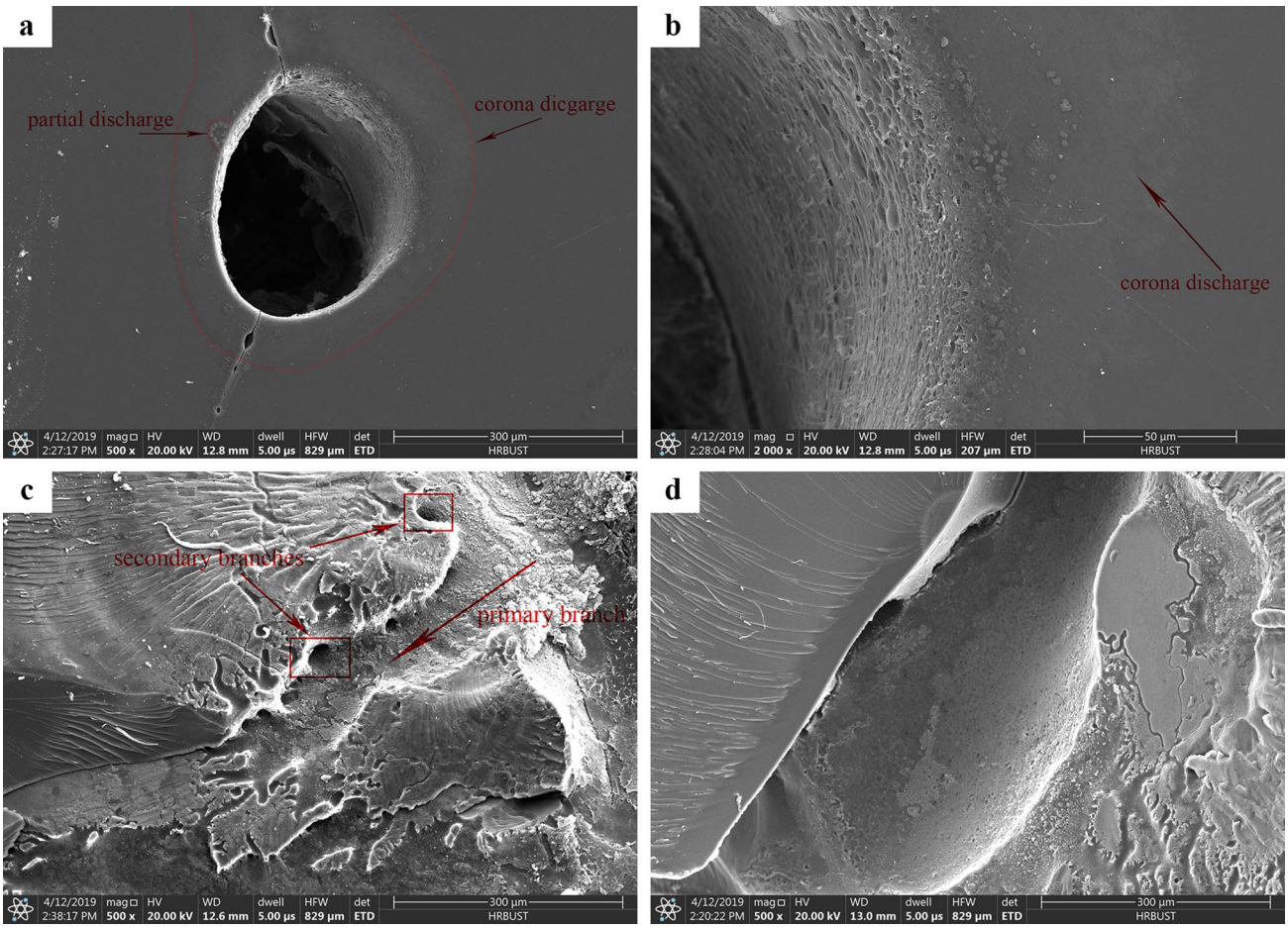


**Fig. 10** SEM images of the breakdown holes: (**a**, **b**) the front of breakdown holes of 3 wt% $Al_2O_3$/E51-BCE, (**c**, **d**) the section of breakdown hole of 3 wt% $Al_2O_3$/E51-BCE and of E51-BCE

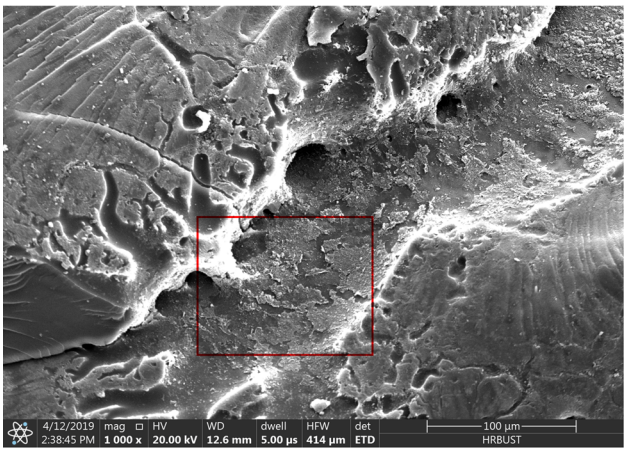


a

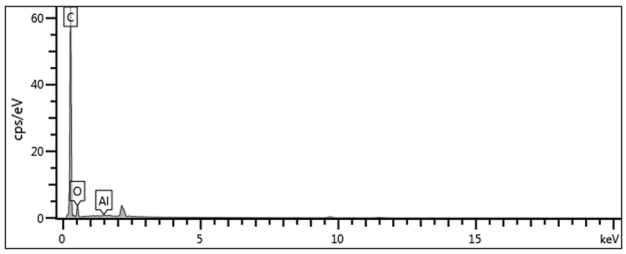


| Element | wt% | at% |
|---|---|---|
| CK | 83.09 | 86.8 |
| OK | 16.7 | 13.1 |
| AlK | 0.22 | 0.1 |
| Matrix | Correction | ZAF |

b

**Fig. 11** SEM image of the breakdown hole branch of 3 wt% $Al_2O_3$/E51-BCE and its EDS spectrum. **a** the branch of breakdown hole **b** EDS spectrum of the branch

**Table 2** Breakdown strength and volume resistivity of $Al_2O_3$/E51-BCE composites

| Component | $Al_2O_3$/wt % | Breakdown strength | | Volume resistivity | |
|---|---|---|---|---|---|
| | | Value/kV $mm^{-1}$ | Increase ratio/ % | Value/$\times 10^{13}$ Ω m | Increase magnification |
| E51-BCE | 0 | 13.3 | – | 1.75 | – |
| $Al_2O_3$/E51-BCE | 1 | 14.3 | 7.5 | 72.5 | 40 |
| $Al_2O_3$/E51-BCE | 3 | 15.1 | 13.5 | 153 | 86 |
| $Al_2O_3$/E51-BCE | 5 | 14.7 | 10.5 | 112 | 63 |

is 13.5% and 86 times higher than that of the matrix resin, respectively. It can be seen that $Al_2O_3$ can significantly improve breakdown strength and the volume resistivity of materials. This is because $Al_2O_3$ can evenly disperse in the E51-BCE matrix resin when the content of $Al_2O_3$ is apposite, and lots of interfaces will be formed between $Al_2O_3$ and the matrix, these interfaces increase trap density inside the composites and make the trap depth deeper. The carriers lose kinetic energy after they collide with $Al_2O_3$ particles during the process of motion [52, 53]; this effect reduces the mobility of carriers and improves the volume resistivity [34]. In the strong electric field, some freely movable carriers inside the medium start to accelerate and bombard the lattices nearby to generate more carriers; finally, a conductive channel is formed internally and the medium loses its insulation properties. Due to the strong interaction of the two phases and hydroxy groups, the incorporated $Al_2O_3$ can enhance the scattering of the carriers and make the composites hard to be broken down [54, 55]. Also, $Al_2O_3$ itself is difficult to generate freely shifting electrons for the covalent bond structure of Al—O is stable, the low concentration of electrons and electron holes will be beneficial to the insulating properties of the composites [56].

## 4 Conclusions

In this paper, the $Al_2O_3$ prepared by sol–gel method is used as a reinforcement to modify E51-BCE matrix resin. The $Al_2O_3$ is short fiber-shaped crystal with hydroxyl groups on its surface, and it has good compatibility with the E51-BCE matrix resin. The thermal decomposition temperature ($T_d$) of the $Al_2O_3$/E51-BCE composites is over 400 °C in the range of 0 ~ 5 wt% $Al_2O_3$; the composite materials still have high heat resistance through the introduction of $Al_2O_3$, slightly decreasing the $T_d$ of the matrix resin. The $Al_2O_3$ also contributes to improving the dielectric properties of the E51-BCE matrix resin. The dielectric constant and dielectric loss tangent of the $Al_2O_3$/E51-BCE composites show peak values of 3.73 and 0.0029 at the electric field frequency of 100 Hz, when the content of $Al_2O_3$ is 5 wt%. And comparing with the E51-BCE matrix resin, the breakdown strength and volume resistivity of the composite materials with 3 wt% $Al_2O_3$ increase by 13.5% and 86 times, respectively.

**Acknowledgements** The authors would like to express their appreciation to the project support by National Natural Science Foundation of

China (Grant No. 51177030) and the Harbin technology bureau subject leader (Grant No. 2015RAXXJ029).

**Data Availability** All data included in this study are available upon request by contact with the corresponding author.

## Compliance with ethical standards

**Conflict of interest** The authors declare that there is no conflict of interests regarding the publication of this paper.

## References


1. S. Zhang, Y.H. Yan, X.D. Li, H.J. Fan, Q.C. Ran, Q. Fu, Y. Gu, Eur. Polym. J. **103**, 124 (2018)
2. Y. Lin, M. Song, React. Funct. Polym. **129**, 58 (2018)
3. J.X. Ma, X.F. Lei, Y.H. Wang, Y.Y. Sun, Iran. Polym. J. **27**, 145 (2018)
4. C.Q. Lu, L. Yuan, Q.B. Guan, G.Z. Liang, A.J. Gu, J. Phys. Chem. C **122**, 5238 (2018)
5. L.C. Gu, G.Z. Liang, Y.P. Shen, A.J. Gu, L. Yuan, Compos. Part B **58**, 66 (2014)
6. L. Yuan, G.Z. Liang, A.J. Gu, Polym. Degrad. Stab. **96**, 84 (2011)
7. L. Tang, J. Dang, M.K. He, J.Y. Li, J. Kong, Y.S. Tang, J.W. Gu, Compos. Sci. Technol. **169**, 120 (2019)
8. C. Uhlig, M. Bauer, J. Bauer, O. Kahle, A.C. Taylor, A.J. Kinloch, React. Funct. Polym. **129**, 2 (2018)
9. A. Zegaoui, M. Derradji, R.K. Ma, W.A. Cai, W.B. Liu, J. Wang, A.Q. Dayo, S. Song, L.L. Zhang, J. Appl. Polym. Sci. **135**, 46283 (2018)
10. F. Wu, B. Song, J. Hah, C.C. Tuan, K.S. Moon, C.P. Wong, J. Polym. Sci. Pol. Chem. **56**, 2412 (2018)
11. F. Wu, C.C. Tuan, B. Song, K.S. Moon, C.P. Wong, J. Polym. Sci. Pol. Chem. **56**, 1337 (2018)
12. C. Zhou, A.J. Gu, G.Z. Liang, L. Yuan, Polym. Adv. Technol. **22**, 710 (2011)
13. L.S. Jayakumari, V. Thulasiraman, M. Sarojadevi, High Perform. Polym. **19**, 33 (2007)
14. F.C. Lü, H.O. Ruan, J.X. Song, K. Yin, Z.Y. Zhan, Y.F. Jiao, Q. Xie, J. Phys. D **52**, 155201 (2019)
15. C. Chen, Y. Xue, X.W. Li, Y.F. Wen, J.W. Liu, Z.G. Xue, D.A. Shi, X.P. Zhou, X.L. Xie, Y.W. Mai, Compos. Part. A **118**, 67 (2019)
16. J.H. Yu, R.M. Huo, C. Wu, X.F. Wu, G.L. Wang, P.K. Jiang, Macromol. Res. **20**, 816 (2012)
17. Z.M. Liu, J.W. Wang, M.Q. Kang, N. Yin, X.K. Wang, Y.S. Tan, Y.L. Zhu, J. Braz. Chem. Soc. **25**, 152 (2013)
18. J. Li, Y.B. Pan, C.S. Xiang, Q.M. Ge, J.K. Guo, Ceram. Int. **32**, 587 (2006)
19. M. Abboud, M. Turner, E. Duguet, M. Fontanille, J. Mater. Chem. **7**, 1527 (1997)
20. X. Sheng, M. Akinc, M.R. Kessler, Polym. Eng. Sci. **50**, 302 (2010)
21. J. Lee, Y. Ko, J. Kim, Macromol. Res. **18**, 200 (2010)
22. B.J. Ash, R.W. Siegel, L.S. Schadler, J. Polym. Sci. Part B **42**(23), 4371–4383 (2004)
23. X.Y. Huang, P.K. Jiang, Y. Yin, Appl. Phys. Lett. **95**, 242905 (2009)
24. G.C. Montanari, D. Fabiani, F. Palmieri, D. Kaempfer, R. Thomann, R. Mulhaupt, I.E.E.E. Trns, Dielectr. Electr. Insul. **11**, 754 (2004)
25. G.L. Wu, K.C. Kou, M. Chao, L.H. Zhuo, J.Q. Zhang, N. Li, Thermochim. Acta **537**, 44 (2012)
26. G.L. Wu, K.C. Kou, M. Chao, L.H. Zhuo, J.Q. Zhang, J. Wuhan Univ. Technol. **28**, 261 (2013)
27. S. Yazman, A. Samanci, Arab. J. Sci. Eng. **44**, 1353 (2019)
28. A.L. Feng, G.L. Wu, C. Pan, Y.Q. Wang, J. Nanosci. Nanotechnol. **17**, 3786 (2017)
29. A.L. Feng, G.L. Wu, Y.Q. Wang, C. Pan, J. Nanosci. Nanotechnol. **17**, 3859 (2017)
30. G.L. Wu, K.C. Kou, L.H. Zhuo, Y.Q. Wang, J.Q. Zhang, Thermochim. Acta **559**, 86 (2013)
31. G.L. Wu, Y.H. Cheng, Q. Xie, C. Liu, K.C. Kou, L.H. Zhuo, Y.Q. Wang, J. Polym. Res. **21**, 615 (2014)
32. S.J. Park, D.I. Seo, J.R. Lee, J. Colloid Interface Sci. **251**, 160 (2002)
33. Z.R. Jia, Z.G. Gao, D. Lan, Y.H. Cheng, G.L. Wu, H.J. Wu, Chin. Phys. B **27**, 117806 (2018)
34. S.Y. Chen, Y.H. Cheng, Q. Xie, B. Xiao, Z.D. Wang, J.Y. Liu, G.L. Wu, Compos. Part A **120**, 84 (2019)
35. J.Y. Lee, Y.G. Liao, R. Nagahata, S. Horiuchi, Polymer **47**, 7970 (2006)
36. M. Venkatesh, S. Gouthaman, S.O. Kanemoto, M.S. Lakshmi, I. Hamerton, J. Appl. Polym. Sci. **136**, 47754 (2019)
37. B.J. Ash, D.F. Rogers, C.J. Wiegand, L.S. Schadler, R.W. Siegel, B.C. Benicewicz, T. Apple, Polym. Compos. **23**, 1014 (2002)
38. Y.Q. Wang, K.C. Kou, W. Zhao, G.L. Wu, F.L. Han, RSC Adv. **5**, 99313 (2015)
39. Y.Q. Wang, K.C. Kou, G.L. Wu, A.L. Feng, L.H. Zhuo, RSC Adv. **5**, 58821 (2015)
40. Y.Q. Wang, G.L. Wu, K.C. Kou, C. Pan, A.L. Feng, J. Mater. Sci. **27**, 8279 (2016)
41. Y.X. Lei, Z.M. Han, D.X. Ren, H. Pan, M.Z. Xu, X.B. Liu, Macromol. Res. **26**, 602 (2018)
42. Y.X. Lei, M.Z. Xu, M.L. Jiang, Y.M. Huang, X.B. Liu, High Perform. Polym. **29**, 1175 (2016)
43. P. Maity, N. Gupta, V. Parameswaran, S. Basu, I.E.E.E. Trns, Dielectr. Electr. Insul. **17**, 1665 (2010)
44. Y.F. Chen, H.Y. Guo, C.B. Geng, Y.Z. Wu, G.Q. Dai, C.J. Teng, J. Mater. Sci. **30**, 991 (2019)
45. Y.Q. Wang, K.C. Kou, G.L. Wu, L.H. Zhuo, J.L. Li, Y. Zhang, Polymer **77**, 354 (2015)
46. L. Wan, X. Zhang, G.L. Wu, A.L. Feng, High Volt. **2**, 167 (2017)
47. R. Popielarz, C.K. Chiang, R. Nozaki, J. Obrzut, Macromolecules **34**, 5910 (2001)
48. S. Singha, M.J. Thomas, I.E.E.E. Trns, Dielectr. Electr. Insul. **16**, 531 (2009)
49. P. Sun, W.X. Sima, X.W. Jiang, D.F. Zhang, J.H. He, L. Ye, High Volt. **4**, 1 (2019)
50. Y.F. Chen, Z.C. Li, J.Y. Tan, Q.Y. Zhang, Y. Han, J. Nanomater. **2015**, 1 (2015)
51. Y.F. Chen, Z.C. Li, C.J. Teng, F.L. Li, Y. Han, J. Electron. Mater. **45**, 6026 (2016)
52. D.L. Ma, R.W. Siegel, J.I. Hong, L.S. Schadler, E. Martensson, C. Onneby, J. Mater. Res. **19**, 857 (2004)
53. N.M. Rashmi, R. Renukappa, N.S. Chikkakuntappa, Kunigal. Polym. Eng. Sci. **51**, 1827 (2011)
54. X.Y. Huang, F. Liu, P.K. Jiang, I.E.E.E. Trns, Dielectr. Electr. Insul. **17**, 1697 (2010)
55. X.H. Zhang, Z.X. Shi, L.S. Ma, J.G. Gao, N. Guo, J. Appl. Polym. Sci. **136**, 47364 (2019)
56. G.L. Wu, Y.H. Cheng, K.K. Wang, Y.Q. Wang, A.L. Feng, J. Mater. Sci. **27**, 5592 (2016)